Sustainable Energy & Fuels

Absorption and Desorption Behaviours of Ammonia on Bis(fluorosulfonyl)amide Salts by the Pressure-Swing Method

Journal:	*Sustainable Energy & Fuels*
Manuscript ID	SE-ART-10-2023-001350.R1
Article Type:	Paper
Date Submitted by the Author:	01-Dec-2023
Complete List of Authors:	Tokushige, Manabu; Chiba University Fujisawa, Ryota; Chiba University Ryu, Junichi; Chiba University,

ARTICLE

Absorption and Desorption Behaviours of Ammonia on Bis(fluorosulfonyl)amide Salts by the Pressure-Swing Method

Manabu Tokushige, Ryota Fujisawa, and Junichi Ryu*

Received 20th October 2023,
Revised 1st December 2023,
Accepted 13th December 2023

DOI: 10.1039/x0xx00000x

The absorption and desorption behaviours of ammonia (NH_3) on bis(fluorosulfonyl)amide (FSA) salts were investigated using the pressure–swing method. The effects of the cation species and temperature of the four types of FSA single salts (Li[FSA], Na[FSA], K[FSA], and Ca[FSA]$_2$) and (Na, K)[FSA] eutectic melt on the NH_3 absorption behaviour were evaluated. FSA salts exhibited large NH_3 storage capacities and the NH_3 absorption behaviour was affected by the different FSA salt cation species. The NH_3 storage capacity increased with decreasing temperature. Although the alkaline metal FSA salts were liquefied by NH_3 absorption at 300 K, Ca[FSA]$_2$ remained solid after NH_3 absorption at 300 K. Additionally, K[FSA] absorbed a lower amount of NH_3 than at 300 K and remained in the solid state after NH_3 absorption at 323 K. These results suggest that NH_3 molecules were dissolved in the FSA salts, and eutectic compounds were formed by NH_3 absorption on the FSA salts. After NH_3 absorption, the salts were found to be composed of ammonium (NH_4^+) cations and amide (NH_2^-) and imide (NH^{2-}) anions.

Introduction

Ammonia (NH_3) technology, cultivated over the past century has benefitted the world by ensuring food availability through its use as a nitrogen-based fertilizer[1,2]. Currently, the widespread use of hydrogen energy makes NH_3 an indispensable energy carrier (transportation medium for hydrogen (H_2))[2–6]. NH_3 has a higher volumetric hydrogen density (121 kg-H_2·m^{-3}) than hydrogen (71 kg-H_2·m^{-3}) and has many advantages as an energy carrier[1–5,7] (Table 1). For example, NH_3 can be readily decomposed into hydrogen[3] or used directly as a fuel[3,6], and its transportation network is already mature[3]. However, conventional production using the Haber-Bosch process requires massive amounts of energy because of the harsh operating conditions including high pressures (20–30 MPa) and temperature (673–873 K), the consumption of fossil fuels, and the release of greenhouse gases[7].

Due to geoenvironmental changes, sustainable NH_3 production must be improved. The authors have focused on NH_3 synthesis using renewable energies[8–10]. For example, nitrogen (N_2) gas can be electrochemically reduced in an ambient environment, while the Haber-Bosch process requires harsh conditions to dissociate the strong N≡N triple bonds[8–10]. Therefore, NH_3 can be synthesised under mild conditions by electrolysis, with competition occurring between H_2 evolution and N_2 reduction[8–10]. Regardless of the synthetic process, NH_3 is usually separated into a cryogenic liquid state at 240 K[11], which requires extensive expensive equipment. Therefore, one of the critical technologies for NH_3 transportation, which is both more efficient and safer, is the separation and storage of NH_3[12–17]. The selective separation and storage of NH_3 lowers the cooling cost because NH_3 is easily collected using the pressure–swing method (PSA). Liu and Aika[13,16,17] confirmed that mixed halide compounds such as $CaCl_2$ and $CaBr_2$ exhibit high storage capacities for NH_3 (the NH_3 storage capacity of $CaCl_2$-$CaBr_2$ (2:1) is 54.1 mmol·g^{-1} at 298 K under 80 kPa by PSA[17]). Additionally, zeolites show high affinity and stability for NH_3 storage (the NH_3 storage capacities of Na-Y and K-Y zeolites are 6.14 and 6.06 mmol·g^{-1}, respectively, at 323 K under 40 kPa by PSA[12,15]). Solid storage of NH_3 has attracted much attention owing to the higher volumetric ammonia density than liquid NH_3[18–20]. Sulfonylamide salts, such as bis(trifluoromethylsulfonyl)amide (TFSA) and bis(fluorosulfonyl)amide (FSA) salts, which are amide salts with imino groups, have several desirable properties, such as nonvolatility and nonflammability[21–23]. Additionally, NH_3 is absorbed by TFSA salts[24,25]. Although FSA salts are expected to absorb NH_3, the absorption and desorption behaviour of NH_3 on FSA salts have not been clarified.

In this study, we investigated the absorption and desorption behaviours of NH_3 on FSA salts. The effects of the cation species and temperature of the four types of FSA single salts (Li[FSA],

Table 1. Various hydrogen carriers[4,7]

Property	NH_3	MeOH	Liq. H_2	Comp. H_2	$LaNi_5$	Mg_2Ni
Hydrogen weight density (*wt*%)	17.6	12.5	100	100	1.4	3.7
Energy density (MWh/m^3)	3.5	4.4	2.4	2.4	–	–
Boiling point (K)	240	338	20	20	–	–

Graduate School of Engineering, Chiba University, Chiba 263-8522 Japan

Na[FSA], K[FSA], and Ca[FSA]$_2$) and (Na, K)[FSA] eutectic melt on NH_3 absorption behaviour were evaluated.

Experimental

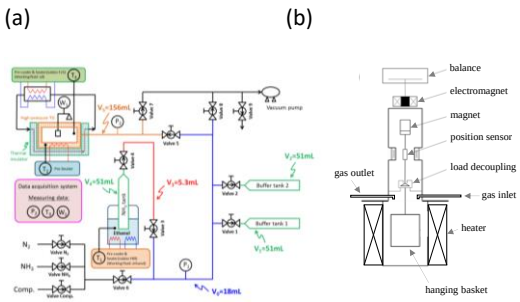

Fig. 1 Experimental setup for NH_3 absorption/desorption cycle examination: (a) gas line and (b) furnace of the magnetic suspension balance.

The NH_3 absorption/desorption cycles of the FSA salts were measured using the PSA with a magnetic suspension balance (MSB-143, Rubotherm GmbH, Germany). Commercially available FSA salts such as Li[FSA] (purity >98%, L0281), Na[FSA](purity >98%, S0992), K[FSA] (purity >95%, P2509), and Ca[FSA]$_2$ (purity >98%, C3476) were purchased from the Tokyo Chemical Industry Co., Ltd. A eutectic mixture ((Na, K)[FSA]=56:41 mol%, melting point; 334 K[23]) was prepared by physically mixing the two salts. The experimental setup is illustrated in Fig. 1. The FSA powder sample was placed in a Pt basket (Ø20 mm×50 mm) hanging from a magnet, and the basket was suspended by a magnetic force inside the furnace. By introducing pure NH_3 gas (99.9% purity, Resonac Holdings Corp., Japan) into the furnace, NH_3 absorption onto the sample was conducted at a NH_3 gas pressure of 0.5 MPa for 2 h (pressure–swing absorption), and the desorption was conducted at a NH_3 gas pressure of 0.1 MPa for 3 h (pressure–swing desorption). The NH_3 gas pressure was controlled by the temperature of the NH_3 tank immersed in an ethanol bath. After the NH_3 absorption/desorption cycles, the sample powders were characterised by X-ray diffraction (XRD; Ultima IV, Rigaku Corp., Japan) and Fourier-transform infrared spectroscopy (FT-IR; FT/IR-4200 spectrometer, JASCO Corp., Japan). XRD data were obtained over the 2θ range of 5–90° at room temperature with a step interval of 0.01° using Cu-*K*α radiation, which was determined by calibrating the Si powder. FT-IR spectra were obtained in the wavenumber range of 4000–400 cm^{-1} in the diffuse reflectance mode in air at room temperature with 128 scans per spectrum at a 4.0 cm^{-1} resolution. The background for FT-IR measurements was calibrated using KBr powder.

Results and discussion

Absorption and desorption behaviours of ammonia

Typical NH_3 absorption/desorption cycles for the Li[FSA] salt at 300 K are shown in Fig. 2. The Li[FSA] showed a stable absorption capacity at both NH_3 gas pressures (0.1 and 0.5 MPa), and the absorption and desorption behaviours of NH_3 on Li[FSA] were observed at 300 K. The absorption and desorption capacities of NH_3 (C_{abs} and C_{des}) are

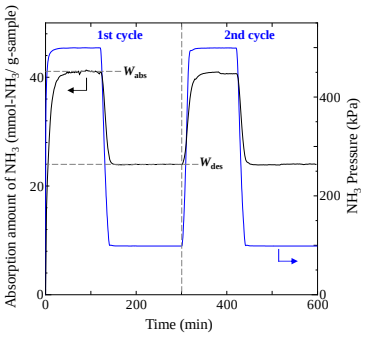

Fig. 2 Typical NH_3 absorption/desorption cycles of Li[FSA] at 300 K.

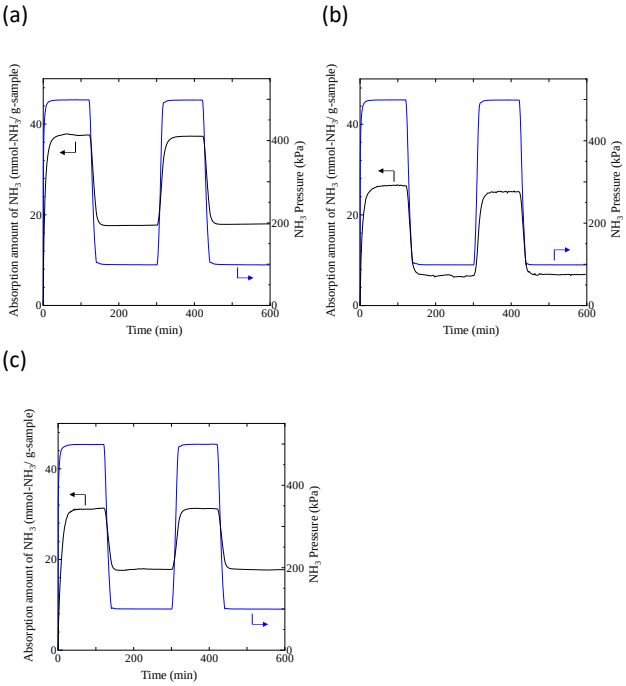

Fig. 3 NH_3 absorption/desorption cycles of each FSA salt at 300 K: (a) Na[FSA], (b) K[FSA], and (c) Ca[FSA]$_2$.

defined as follows:

$$C_{abs} = \frac{W_{abs} - W_S}{W_S} \quad (1)$$

$$C_{des} = \frac{|W_{des} - W_{abs}|}{W_S} \quad (2)$$

where W_S is the sample weight before the NH_3 absorption/desorption cycle, W_{abs} is the sample weight after the absorption cycle, and W_{des} is the sample weight after the desorption cycle. Furthermore, the absorption and desorption rates (v_{abs} and v_{des}) were defined as the rates at which 80% of the capacity was achieved in each cycle. Li[FSA] exhibited the highest NH_3 storage capacity (C_{abs} =41.2 mmol·g^{-1}) among the four single FSA salts, and the NH_3 absorption behaviour was affected by the different cation species of

Table 2. Results of NH_3 absorption/desorption measurements at 300 K

FSA	Cycle	Absorption Capacity, C_{abs} (mmol·g^{-1})	Absorption rate, v_{abs} (mmol·g^{-1}·min^{-1})	Desorption Capacity, C_{des} (mmol·g^{-1})	Desorption rate, v_{des} (mmol·g^{-1}·min^{-1})
Li[FSA]	1st 2nd	41.2 40.7	2.95 2.23	17.2 16.7	0.81 0.79
Na[FSA]	1st 2nd	37.6 37.3	3.48 1.90	19.9 19.3	0.84 0.80
K[FSA]	1st 2nd	26.4 25.2	1.95 1.12	19.8 18.4	0.89 0.83
$Ca[FSA]_2$	1st 2nd	31.35 30.54	1.79 1.62	14.2 13.4	0.57 0.54

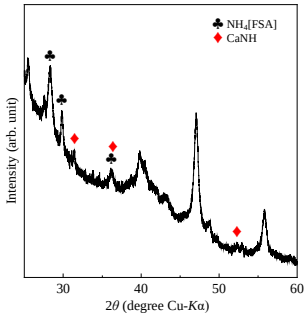

Fig. 4 XRD pattern of the $Ca[FSA]_2$ sample after NH_3 absorption/ desorption examination at 300 K.

the FSA salts (Fig. 3). This result was consistent with that of Liu and Aika[15]. They identified the absorption site of NH_3 and clarified the absorption mechanism on alkaline or alkaline earth metal cations using a thermal conductivity detector and FT-IR spectroscopy. NH_3 absorbs on these cations by three processes: Coulombic attraction, the formation of ammonium ions, and the formation of ammine complexes on cation sites. Therefore, it was suggested that NH_3 absorbs on alkaline or alkaline earth metal cations in FSA salts. The results of the NH_3 absorption/desorption cycles for each FSA sample at 300 K are summarised in Table 2. After the NH_3 absorption/desorption cycles, the solid Li[FSA] was liquefied. This liquefaction was also observed for Na[FSA] and K[FSA]. $Ca[FSA]_2$ remained in the solid state, and was composed of $NH_4[FSA]$[26] and CaNH[27] phases (Fig. 4), indicating that NH_3 was dissolved in the FSA salt. The dissolution mechanism of NH_3 in the FSA salt is discussed at the end of this section. The C_{abs} values increased in the order Li[FSA] > Na[FSA] > $Ca[FSA]_2$ > K[FSA]. According to the results of Liu and Aika[15], NH_3 molecules are absorbed by the Coulombic attraction between alkaline or alkaline earth metal cations and nitrogen anions of NH_3. Therefore, the C_{abs} varies with the surface charge density of the alkaline or alkaline earth metal cations. Despite the Ca^{2+} cation having the highest surface charge density among the cations used in this study, Li[FSA] and Na[FSA] showed higher C_{abs} values than $Ca[FSA]_2$. This can be attributed to the different physical states of the FSA salts. Liquid FSA salt shows higher C_{abs} value than solid one. Regarding the kinetics, the NH_3 absorption rates (v_{abs}) of the alkaline metal FSA salts of 1st cycle differed from those of 2nd cycle due of the different physical state of the FSA salt. NH_3 molecules were absorbed on the solid FSA salt during the 1st cycle and on the liquid FSA salt after the 1st cycle. Solid powder FSA salts rapidly absorbed the NH_3 molecules owing to the high surface area.

To evaluate the temperature dependency of the NH_3 absorption and desorption behaviours on FSA salts, NH_3 absorption/desorption

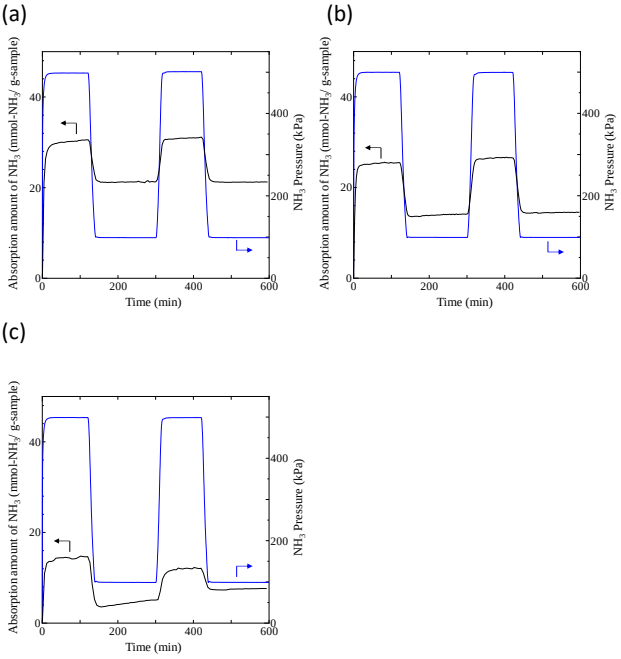

Fig. 5 NH_3 absorption/desorption cycles of each FSA salt at 323 K. (a) Li[FSA], (b) Na[FSA], and (c) K[FSA]

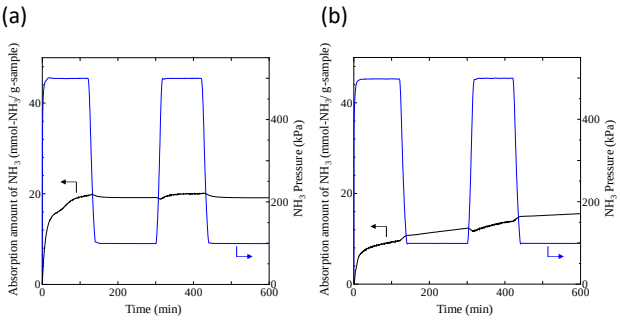

Fig. 6 NH_3 absorption/desorption cycles of each FSA salt at 373 K. (a) Na[FSA] and (b) K[FSA]

cycles were conducted at 323 K and 373 K and are shown in Figs. 5 and 6. The C_{abs} values decreased as the temperature increased owing to the vigorous motion of the NH_3 molecules. The NH_3 absorption/desorption cycle results for each FSA sample at 323 K are summarised in Table 3. A small amount of the absorbed NH_3 was desorbed from Na[FSA], and the desorption behaviour of the absorbed NH_3 was not observed on K[FSA] at 373 K, which was close to the melting point (Na[FSA]: 379 K and K[FSA]: 375 K)[24]. Figure 7 shows the NH_3 absorption/desorption curves on the (Na, K)[FSA] eutectic melt at 373 K. Even on the (Na, K)[FSA] melt, the desorption behaviour of the absorbed NH_3 was not observed. These results indicated that the desorption of the absorbed NH_3 was lower in the liquid state than that in the solid state due of the low surface area. After the NH_3 absorption/desorption cycle at 323 K, although solid Li[FSA] and Na[FSA] were liquefied, K[FSA] remained in the solid state. However, the v_{abs} value of the K[FSA] salt in 1st cycle differed from that in 2nd cycle, which suggested that this salt was liquid-state under high NH_3 pressure and was solidified with release of dissolved

NH_3 at ambient pressure. These results indicated that a eutectic compound was formed by NH_3 absorption on FSA salt. Although NH_3 was absorbed on K[FSA] until the liquidus composition at 300 K, it remained in the solidus composition owing to the less absorbed NH_3 at 323 K. The XRD patterns and FT-IR spectra of the K[FSA] samples before and after the NH_3 absorption/desorption cycle are shown in Fig. 8. The observed diffraction pattern of the sample before the NH_3 absorption/desorption cycle was assigned to K[FSA] with an orthorhombic *Pcab* structure[28]. On the other hand, the sample after the NH_3 absorption/desorption cycle was composed of NH_4[FSA][26] and KNH_2[29] phases. The FT-IR peaks could be attributed to N–H bonds from not only the ammonium cation (NH_4^+)[30] but also from the amide

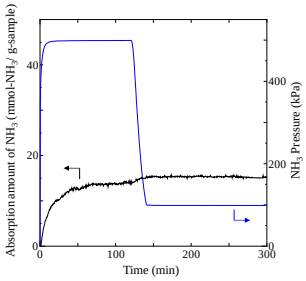

Fig. 7 NH_3 absorption/desorption cycles of the (Na, K)[FSA] eutectic melt at 373 K.

(a) (b)

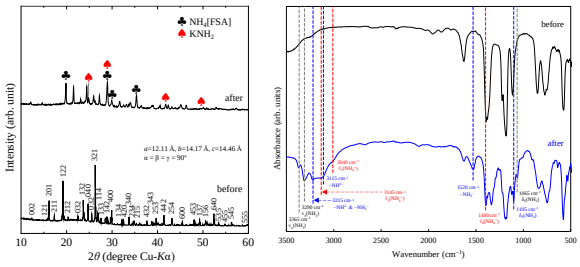

Fig. 8 XRD patterns (a) and IR spectra (b) of the K[FSA] sample before and after NH_3 absorption/desorption at 323 K.

Table 3. Results of NH_3 absorption/desorption measurements at 323 K

FSA	Cycle	Absorption Capacity, C_{abs} (mmol·g^{-1})	Absorption rate, v_{abs} (mmol·g^{-1}·min^{-1})	Desorption Capacity, C_{des} (mmol·g^{-1})	Desorption rate, v_{des} (mmol·g^{-1}·min^{-1})
Li[FSA]	1st 2nd	30.6 31.1	3.98 2.34	9.29 9.84	0.42 0.43
Na[FSA]	1st 2nd	25.5 26.5	3.50 1.64	11.3 12.0	0.50 0.51
K[FSA]	1st 2nd	14.6 12.1	1.63 0.53	9.52 4.48	0.53 0.23

(NH_2^-)[30–32] and imide (NH^{2-})[30] anions. Therefore, NH_3 was dissolved in K[FSA] as follows:

$$K[FSA] + 2NH_3 \rightarrow NH_4[FSA] + KNH_2 \quad (3)$$

$$K[FSA] + KNH_2 + NH_3 \rightarrow NH_4[FSA] + K_2NH \quad (4)$$

$$2KNH_2 \rightarrow K_2NH + NH_3 \quad (5)$$

These reactions were consistent with the results of Ichikawa et al. [33,34] The liquefaction of solid salts excessively absorbing NH_3 was already reported[35]. This liquefaction can be explained by a eutectic phenomenon with ammonium salt. In this study, NH_4[FSA] was formed by absorption of NH_3 on FSA salt, and was liquefied by eutectic among them. For example, NH_4[FSA] was formed with absorption of NH_3 on K[FSA] salt by reaction (3), (K, NH_4)[FSA] eutectic melt was generated and was liquefied. Additionally, Serizawa et al.[36,37] observed that NH_3 was dissolved in chloride salt as NH_2^- and NH^{2-} anions using FT-IR spectroscopy. Therefore, NH_2^- and NH^{2-} compounds were formed in equilibria between FSA salt and NH_3 under high NH_3 pressure by reactions (4) and (5), and might be

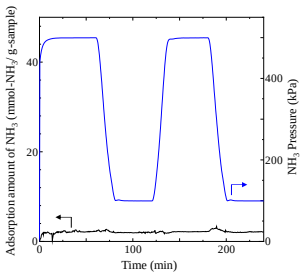

Fig. 9 NH_3 adsorption/desorption cycles of Na-Y zeolite at 300 K.

involved in the eutectic phenomenon between K[FSA] and NH_4[FSA]. The above results found that NH_3 was dissolved in FSA salt as NH_4^+ cations and NH_2^- and NH^{2-} anions.

Comparison of FSA salts with zeolites

In our previous study[38], the NH_3 adsorption/desorption behaviours on zeolites in the PSA cycle (0.1–0.5 MPa) at 473 K were observed, and their stabilities for NH_3 storage were confirmed. Zeolites are commonly used NH_3 adsorbents at room temperature. Typical NH_3 adsorption and desorption behaviours on Na-Y zeolite at 300 K are shown in Fig. 9. For the Na-Y zeolite, the NH_3 adsorption capacity (C_{ads}=2.25 mmol·g^{-1}, 3.17 mol·m^{-3}) was much lower than that of the Na[FSA] salt (C_{abs} =37.6 mmol·g^{-1}, 88.9 mol·m^{-3}). Moreover, the adsorbed NH_3 was not desorbed at 300 K. Additionally, the NH_3 desorption rate for Na-Y zeolite (v_{des}=0.55 mmol·g^{-1}·min^{-1}) was significantly slower than that of the Na[FSA] salt (v_{des} =3.48 mmol·g^{-1}·min^{-1}). Therefore, zeolites are unsuitable NH_3 storage materials for PSA cycles. The advantage of zeolites is their low cost. FSA salts are not industrially mass-produced, and their prices are approximately 80 times higher than those of zeolites. The industrial production of FSA salts is required for their use as room-temperature NH_3 storage materials.

Conclusions

The absorption and desorption behaviours of NH_3 on FSA salts were observed using the PSA. The effects of their cation species and temperature of four types of FSA single salts (Li[FSA], Na[FSA], K[FSA], and Ca[FSA]$_2$) and (Na, K)[FSA] eutectic melt on NH_3 absorption behaviour were evaluated. The storage capacity of NH_3

increased in the order Li[FSA] > Na[FSA] > $Ca[FSA]_2$ > K[FSA]. Although the alkaline metal FSA salts were liquefied by NH_3 absorption at 300 K, $Ca[FSA]_2$ remained solid after NH_3 absorption at 300 K. At 323 K, K[FSA] absorbed a lower amount of NH_3 than at 300 K and remained in the solid state after NH_3 absorption. The solid FSA salts were composed of ammonium (NH_4^+) cations as well as amide (NH_2^-) and imide (NH^{2-}) anions after NH_3 absorption. Therefore, NH_2^- and NH^{2-} anions were formed in equilibria between FSA salt and NH_3 under high pressure, and solid FSA salt was liquified by eutectic among them. This study found that NH_3 was dissolved in FSA salt as NH_4^+ cations and NH_2^- and NH^{2-} anions.

Author Contributions

M.T.: Investigation, Data Curation, Visualization, Writing-Original draft. R.F.: Investigation, Data Curation J.R.: Supervision, Funding acquisition, Writing-Review and Editing, Revision and Suggestions. All the authors participated in discussions of the results and in preparing the manuscript.

Conflicts of interest

There are no conflicts to declare.

Acknowledgements

This research was supported by the Science and Technology Research Partnership for Sustainable Development (SATREPS) in collaboration with the Japan Science and Technology Agency (JST, JPMJSA2104) and the Japan International Cooperation Agency (JICA). The authors gratefully acknowledge support provided by the Research Foundation. We would also like to thank Mr. Shun Mashiko and Mr. Morihiro Suzuki for their work on the preliminary experiments.

References

1 J.W. Erisman, M.A. Sutton, J. Galloway, Z. Klimont, W. Winiwarter, *Nature Geosci*., 2008, **1**, 636.
2 D.R. MacFarlane, P.V. Cherepanov, J. Choi, B.H.R. Suryanto, R.Y. Hodgetts, J.M. Bakker, F.M.F. Vallana, A.N. Simonov, *Joule*, 2020, **4**, 1186.
3 A. Valera-Medina, H. Xiao, M. Owen-Jones, W.I.F. David, P.J. Bowen, *Prog. Energy Combust. Sci*., 2018, **69**, 63.
4 R. Lan, K.A. Alkhazmi, I.A. Amar, S. Tao, *Appl. Cat. B*, 2014, **152–153**, 212.
5 K.E. Lamb, M.D. Dolan, D.F. Kennedy, *Int. J. Hydrog. Energy*., 2019, **44**, 3580.
6 Y. Zhao, B.P. Setzler, J. Wang, J. Nash, T. Wang, B. Xu, Y. Yan, *Joule*, 2019, **3**, 2472.
7 F.J. Desai, M.N. Uddin, M.M. Rahman, R. Asmatulu, *Int. J. Hydrog. Energy*, 2023, **48**, 29256.
8 S. Giddey, S.P.S. Badwal, A. Kulkarni, *Int. J. Hydrog. Energy*, 2023, **38**, 14576.
9 Q. Wang, J. Guo, P. Chen, *J. Energy Chem*., 2019, **36**, 25.
10 A.G. Olabi, M. Abdelkareem, M. Al-Murisi, N. Shehata, A. Alami, A. Radwan, T. Wilberforce, K. Chae, E.T. Sayed, *Energy Convers. Manag*., 2023, **277**, 116594
11 H. Liu, Chin. *J. Catal*., 2014, **35**, 1619.
12 C.Y. Liu, K. Aika, *Res. Chem. Intermed*., 2002, **28**, 409.
13 C.Y. Liu, K. Aika, *Chem. Lett*., 2002, **31**, 798.
14 C.Y. Liu, K. Aika, *Bull. Chem. Soc. Jpn*. 2003, **76**, 1463.
15 C.Y. Liu, K. Aika, *J. Jpn. Petrol. Inst*., 2003, **46**, 301.
16 C.Y. Liu, K. Aika, *Bull. Chem. Soc. Jpn*., 2004, **77**, 123.
17 C.Y. Liu, K. Aika, *Indust. Eng. Chem.Res*. 2004, **43**, 7484.
18 T. Zhang, H. Miyaoka, H. Miyaoka, T. Ichikawa, Y. Kojima, *ACS Appl. Energy Mater*., 2018, **1**, 232.
19 T.D. Elmøe, R.Z. Sørensen, U. Quaade, C.H. Christensen, J.K. Nørskov, T. Johannessen, *Chem. Eng. Sci*., 2006, 61, 2618.
20 A. Klerke, C.H. Christensen, J.K. Nørskov, T. Vegge, *J. Mater. Chem*., 2008, **18**, 2304.
21 J. Foropoulos, D.D. DesMarteau, *J. Am. Chem. Soc*., 1982, **1040**, 4260.
22 J. Foropoulos, D.D. DesMarteau, *J. Fluorine Chem*., 1982, **21**, 9.
23 K. Kubota, T. Nohira, R. Hagiwara, *J. Chem. Eng. Data*, 2010, **55**, 3142.
24 A. Yokozeki, M.B. Shiflett, *Applied Energy*, 2007, **84**, 1258.
25 A. Yokozeki, M.B. Shiflett, *Ind. Eng. Chem. Res*., 2007, **46**, 1605.
26 J. Tang, Z. Zhou, M. Chen, R. Wang, L. Song, International patent, WO2022053002A1
27 H.H. Franck, M.A. Bredig, G. Hoffmann, *Naturwissenschaften*, 1933, **21**, 330.
28 K. Matsumoto, T. Oka, T. Nohira, R. Hagiwara, *Inorg. Chem*., 2013, **52**, 568.
29 R. Juza, H. Liedtke, *Zeitschrift fuer anorganische und allgemeine chemie*, 1957, **290**, 204.
30 K. Nakamoto, Infrared and Raman Spectra of Inorganic and Coordination Compounds (6th Edition) Part B: Applications in Coordination, Organometallic, and Bioinorganic Chemistry, Wiley, NJ, 2009.
31 J.P.O. Bohger, R.R. Eßmann, H. Jacobs, *J. Mol. Struct*., 1995, **348**, 325.
32 P. Botschwina, *J. Mol. Spect*., 1986, **117**, 173.
33 T. Ichikawa, N. Hanada, S. Isobe, H. Leng, H. Fujii, *J. Phys. Chem. B*, 2004, **108**, 7887.
34 S. Isobe, T. Ichikawa, S. Hino, H. Fujii, *J. Phys. Chem. B*, 2005, **109**, 14855.
35 L. Gao, H. Fang, Z. Li, Yu, K. Fan, *Inorg. Chem*., 2011, **50**, 4301.
36 N. Serizawa, H. Miyashiro, K. Takei, T. Ikezumi, T. Nishikiori, Y. Ito, *J. Electrochem. Soc*., 2012, **159**, E87.
37 N. Serizawa, K. Takei, T. Nishikiori, Y. Katayama, Y. Ito, *Electrochemistry*, 2018, **86**, 88.
38 M. Tokushige, J. Ryu, *ACS Omega*, 2023, **8**, 32536.